A Theoretical Examination of the Acid-Catalyzed and Noncatalyzed Ring-Opening Reaction of an Oxirane by Nucleophilic Addition of Acetate. Implications to Epoxide Hydrolases

Edmond Y. Lau, Zachary E. Newby, and Thomas C. Bruice*

Contribution from the Department of Chemistry and Biochemistry, University of California, Santa Barbara, California 93106

Received October 24, 2000

Abstract: Ab initio and density functional calculations have been performed to gain a better understanding of the epoxide ring-opening reaction catalyzed by epoxide hydrolase. The S_N2 reaction of acetate with 1*S*,2*S*-*trans*-2-methylstyrene oxide to provide the corresponding diol acetate ester was studied with and without general-acid catalysis. MP2 and DFT (B3LYP) calculations predict, for the noncatalyzed reaction, a central barrier of approximately 20−21 kcal/mol separating the reactants from products depending on which carbon center in the epoxide is undergoing attack. From these gas-phase reactions the immediate alkoxide products are not energetically far below their associated transition states such that the reaction is predicted to be endothermic. Inclusion of aqueous solvation effects via a polarizable continuum model predicts the activation barrier to increase by almost 10 kcal/mol due to the solvation of the acetate ion nucleophile. The activation barrier for the epoxide ring-opening reaction is reduced to ∼10 kcal/mol when phenol, as the general-acid catalyst, is included in the gas-phase calculations. This is due to the immediate product being the neutral ester rather than the corresponding alkoxide. The transition state in the general-acid-catalyzed reaction is earlier than that for the noncatalyzed reaction and the reaction is highly exothermic. Molecular mechanics calculations of 1*S*,2*S*-*trans*-2-methylstyrene oxide in the active site of murine epoxide hydrolase show two possible binding conformations. Both conformers have the epoxide oxygen forming hydrogen bonds with the acidic hydrogens of the catalytic tyrosines (Tyr381 and Tyr465). These two conformations likely lead to different products since the nucleophile (Asp333-CO_2^-) is positioned to react with either carbon center in the epoxide.

Introduction

Epoxide hydrolases have recently been shown to exist in a wide variety of organisms from insects to fungi, bacteria, plants, and mammals.[1,2] Epoxide hydrolases catalyze the conversion of epoxides to more soluble and easily excretable vicinal diols. These ubiquitous enzymes are vital to the process of detoxification in living cells.[1,2] Epoxides, which can be carcinogenic and mutagenic, are formed in liver cells in the course of detoxification of some xenobiotics. In mammals there are two major forms of epoxide hydrolases: microsomal (mEH) and soluble (sEH). The soluble form is found in the cytosol and the perioxisomal matrix of liver cells while the microsomal form is membrane anchored.[3] The two forms of epoxide hydrolase have low sequence homology. In addition, the reactivity and specificity differs between the two forms of epoxide hydrolase.[4] Epoxide hydrolases function optimally in the pH range 6.5 to 9.0 depending on the form.[4,5]

Hydrolysis of an oxirane by epoxide hydrolase occurs in two steps (Scheme 1).[6] Cofactors or metal ions are not needed for enzymatic activity. The first step in the reaction involves formation of an ester intermediate via S_N2 attack by a Asp-CO_2^- on epoxide anti to the epoxide oxygen.[7] The reaction is assisted by general-acid catalysis involving phenolic hydrogens of two tyrosines in the active site.[8,9] The diol is formed in the second step of the reaction by hydrolysis of the ester intermediate. The nucleophilic water is activated by being a member of a water−histidine−aspartate triad. Hydrolysis of the ester intermediate is the rate-limiting step in this reaction.[10,11] The alkylation reaction is 10^2-10^3 faster than the hydrolysis.[8,12] The features of aspartate nucleophilic attack on substrate to form an ester and rate determining hydrolysis of ester by water as part of a Asp-His-H_2O triad closely resemble the haloalkane dehalogenase mechanism.[13]

So far, the crystal structures of three different epoxide hydrolases have been solved. Although the enzymes came from different sources (*Agrobacterium radiobactor*, *Aspergillus niger*,

* Author to whom correspondences should be addressed. Phone: (805) 893-2044. Fax: (805) 893-2229. E-mail: tcbruice@bioorganic.ucsb.edu.

(1) Archer, I. V. J. *Tetrahedron* **1997**, *53*, 15617−15662.
(2) Orru, R. A. V.; Faber, K. *Curr. Opin. Chem. Biol.* **1999**, *3*, 16−21.
(3) Arand, M.; Grant, D. F.; Beetham, J. K.; Friedberg, T.; Oesch, F.; Hammock, B. D. *FEBS Lett.* **1994**, *338*, 251−256.
(4) Ota, K.; Hammock, B. D. *Science* **1980**, *207*, 1479−1481.
(5) Meijer, J.; Depierre, J. W. *Eur. J. Biochem.* **1985**, *150*, 7−16.
(6) Arand, M.; Wagner, H.; Oesch, F. *J. Biol. Chem.* **1996**, *271*, 4223−4229.
(7) Lacourciere, G. M.; Armstrong, R. N. *J. Am. Chem. Soc.* **1993**, *115*, 10466−10467.
(8) Rink, R.; Kingma, J.; Lutje Spelberg, J. H.; Jannsen, D. B. *Biochemistry* **2000**, *39*, 5600−5613.
(9) Yamada, T.; Morisseau, C.; Maxwell, J. E.; Argiriadi, M. A.; Christianson, D. W.; Hammock, B. D. *J. Biol. Chem.* **2000**, *275*, 23082−23088.
(10) Tzeng, H.-F.; Laughlin, L. T.; Lin, S.; Armstrong, R. N. *J. Am. Chem. Soc.* **1996**, *118*, 9436−9437.
(11) Rink, R.; Janssen, D. B. *Biochemistry* **1998**, *37*, 18119−18127.
(12) Tzeng, H.-F.; Laughlin, L. T.; Armstrong, R. N. *Biochemistry* **1998**, *37*, 2905−2911.
(13) Verschueren, K. H. G.; Seljee, F.; Rozeboom, H. J.; Kalk, K. H.; Dijkstra, B. W. *Nature* **1993**, *363*, 693−698.

10.1021/ja0037724 CCC: $20.00
Published on Web 03/16/2001

Scheme 1

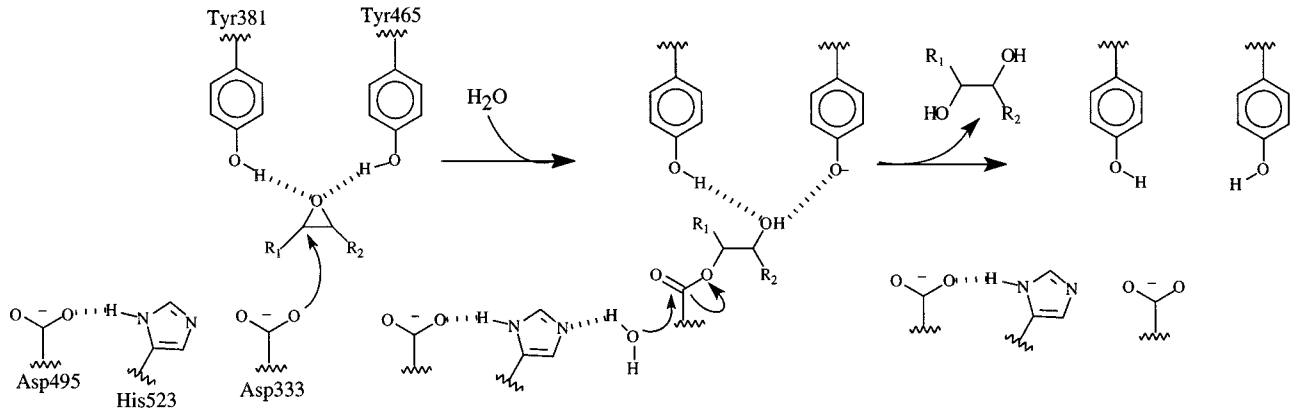

and murine), the active sites of the three enzymes are remarkably similar.[14−16] There are two tyrosines which are positioned to form hydrogen bonds with the epoxide and in all three structures and the nucleophile is aspartic acid. The only mammalian crystal structure of an epoxide hydrolase is that of murine epoxide hydrolase.[15] The enzyme is a homodimer with each unit consisting of 544 residues. The overall structure of the monomer consists of two compact domains which are joined together by a meandering strand. The N-terminus is the vestigial domain (Arg4-Gly218) and the C-terminus contains the catalytic domain (Val235-Ala544). The C-terminus adopts an α/β hydrolase fold. The haloalkane dehalogenase and both forms of epoxide hydrolase are part of the α/β hydrolase fold family and thought to have evolved from a common ancestor.[3] Asp333 is the catalytic nucleophile and positioned at the end of a loose 25 Å deep "L" shaped cavity. Tyr381 and Tyr465 are conserved in all sEH and Tyr465 is conserved in all epoxide hydrolases. Studies of mutants of murine and *Agrobacterium radiobactor* epoxide hydrolases have shown that one of the tyrosines can be replaced with a phenylalanine without loss of catalytic activity.[8,9] The rate of ester formation (k_2) of chalcone oxides by mutant murine sEH (Y381F and Y465F) was approximately (2−30)-fold decreased relative to the wild-type enzyme.[9] It should be pointed out that chalcone oxides are poor substrates for epoxide hydrolases and form stable covalent intermediates. When both tyrosines are replaced with phenylalanines the enzyme is inactive. Mutants of *Agrobacterium radiobactor* epoxide hydrolase (Y215F and Y152F) show a similar behavior. The rate of ester formation (k_2) for (*S*)-styrene oxide with the Y215F mutant was 20-fold slower than that with the wild-type enzyme.

To gain insight into the S_N2 ester formation reaction catalyzed by epoxide hydrolase, ab initio and density functional theory (DFT) calculations were performed on model systems with and without phenol general-acid catalysis. Molecular mechanics calculations with the crystal structure of murine epoxide hydrolase were used to determine possible binding conformations for the substrate 1*S*,2*S*-*trans*-2-methylstyrene oxide (tMSO) in the active site.

Method

The first step in the hydrolysis of an oxirane compound by murine epoxide hydrolase has been investigated by using quantum mechanical calculations. The nucleophilic Asp333 was represented by acetate and the substrate employed is 1*S*,2*S*-*trans*-2-methylstyrene oxide (tMSO), which is a good substrate for rodent sEH.[4] All quantum mechanical calculations were performed with the programs Gaussian 94 and 98.[17,18] Geometry optimizations for the noncatalyzed reaction were performed at the HF/6-31+G(d,p) and B3LYP/6-31+G(d,p)[19,20] levels of theory. Harmonic frequency calculations were performed on all optimized structures. The zero-point vibrational energies (ZPE) were scaled by 0.893 for HF calculations and 0.980 for DFT calculations.[21,22] Transition states for the epoxide ring opening were calculated for phenyl side and methyl side attack by acetate. Transition states were characterized by a single imaginary frequency. Although the B3LYP method includes the effects of electron correlation, it can underestimate the activation barrier.[23,24] The effects of electron correlation were further assessed by single-point MP2/6-31+G(d,p) calculations on the HF/6-31+G(d,p) geometries.

Single-point aqueous solvation calculations were performed with Gaussian 98 on the optimized DFT geometries using a polarizable continuum model (COSMO/CPCM) to estimate the influence of solvation (water, $\epsilon = 78.39$) on this reaction.[25] It has been shown that the solvation free energies obtained from single-point PCM calculations with gas-phase geometries from DFT calculations are in reasonable agreement with the values from full geometry optimizations.[26,27] All

(14) Nardini, M.; Ridder, I. S.; Rozeboom, H. J.; Kalk, K. H.; Rink, R.; Janssen, D. B.; Dijkstra, B. W. *J. Biol. Chem.* **1999**, *274*, 14579−14586.
(15) Argiriadi, M. A.; Morisseau, C.; Hammock, B. D.; Christianson, D. W. *Proc. Natl. Acad. Sci. U.S.A.* **1999**, *96*, 10637−10642.
(16) Zou, J.; Hallberg, B. M.; Bergfors, T.; Oesch, F.; Arand, M.; Mowbray, S. L.; Jones, T. A. *Structure* **2000**, *8*, 111−122.
(17) Frisch, M. J.; Trucks, G. W.; Schlegel, H. B.; Gill, P. M. W.; Johnson, B. G.; Robb, M. A.; Cheeseman, J. R.; Keith, T.; Petersson, G. A.; Montgomery, J. A.; Raghavachari, K.; Al-Laham, M. A.; Zakrzewski, V. G.; Ortiz, J. V.; Foresman, J. B.; Cioslowski, J.; Stefanov, B. B.; Nanayakkara, A.; Challacombe, M.; Peng, C. Y.; Ayala, P. Y.; Chen, W.; Wong, M. W.; Andres, J. L.; Replogle, E. S.; Gomperts, R.; Martin, R. L.; Fox, D. J.; Binkley, J. S.; Defrees, D. J.; Baker, J.; Stewart, J. P.; Head-Gordon, M.; Gonzalez, C.; Pople, J. A. *Gaussian 94*, Revision D.4 ed.; Gaussian, Inc.: Pittsburgh, PA, 1995.
(18) Frisch, M. J.; Trucks, G. W.; Schlegel, H. B.; Scuseria, G. E.; Robb, M. A.; Cheeseman, J. R.; Zakrzewski, V. G.; Montgomery, J. A.; Stratmann, R. E.; Burant, J. C.; Dapprich, S.; Millam, J. M.; Daniels, A. D.; Kudin, K. N.; Strain, M. C.; Farkas, O.; Tomasi, J.; BaroneV.; Cossi, M.; Cammi, R.; Mennucci, B.; Pomelli, C.; Adamo, C.; Clifford, S.; Ochterski, J.; Petersson, G. A.; Ayala, P. Y.; Cui, Q.; Morokuma, K.; Malick, D. K.; Rabuck, A. D.; Raghavachari, K.; Foresman, J. B.; Cioslowski, J.; Ortiz, J. V.; Stefanov, B. B.; Liu, G.; Liashenko, A.; Piskorz, P.; Komaromi, I.; Gomperts, R.; Martin, R. L.; Fox, D. J.; Keith, T.; Al-Laham, M. A.; Peng, C. Y.; Nanayakkara, A.; Gonzalez, C.; Challacombe, M.; Gill, P. M. W.; Johnson, B.; Chen, W.; Wong, M. W.; Andres, J. L.; Gonzalez, C.; Head-Gordon, M.; Replogle, E. S.; Pople, J. A. *Gaussian 98*, revision A.6 ed.; Gaussian, Inc.: Pittsburgh, PA, 1998.
(19) Becke, A. D. *J. Chem. Phys.* **1993**, *98*, 5648−5652.
(20) Lee, C.; Yang, W.; Parr, R. G. *Phys. Rev. B* **1988**, *37*, 785−789.
(21) Pople, J. A.; Scott, A. P.; Wong, M. W.; Radom, L. *Isr. J. Chem.* **1993**, *33*, 345−350.
(22) Wong, M. W. *Chem. Phys. Lett.* **1996**, *256*, 391−399.
(23) Bach, R. D.; Glukhovtsev, M. N.; Gonzalez, C.; Marquez, M.; Estevez, C. M.; Baboul, A. G.; Schlegel, H. B. *J. Phys. Chem. A* **1997**, *101*, 6092−6100.
(24) Laitinen, T.; Rouvinen, J.; Perakyla, M. *J. Org. Chem.* **1998**, *63*, 3, 8157−8162.
(25) Klamt, A.; Schuurmann, G. *J. Chem. Soc., Perkins Trans. 2* **1993**, *5*, 799−805.
(26) Barone, V.; Cossi, M.; Tomasi, J. *J. Comput. Chem.* **1998**, *19*, 404−417.

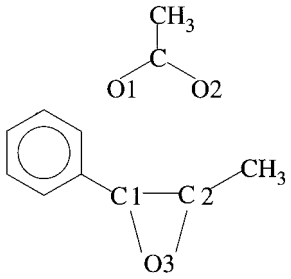

Figure 1. Atom numbering used for acetate and tMSO in the text.

solvation calculations used the united atom model for Hartree−Fock (UAHF) parameters and 60 tesserae for the cavity.[26,28]

To determine the effect of a general-acid catalyst on this epoxide ring-opening reaction, a single phenol was included in the calculation to mimic the effect of either active site Tyr381 or Tyr465 interacting with tMSO. The various stationary points for acetate and tMSO from the HF/6-31+G(d,p) calculations were used to generate initial coordinates for the acid-catalyzed reaction by modeling each structure into the active site of the murine epoxide hydrolase. The coordinates of acetate, tMSO, and the side chain of the closest tyrosine (Tyr381) to the epoxide oxygen were saved and used for further calculations. The initial structures were optimized by using the PM3 semiempirical Hamiltonian.[29] The final structures from the PM3 optimization were used for ab initio calculations at the HF/6-31+G(d) level of theory. Single-point energies were calculated at the MP2/6-31+G(d,p) and B3LYP/6-31+G(d,p) levels of theory from the HF/6-31+G(d) geometries to determine the effects of electron correlation on this reaction.

An estimate of the binding conformation of the 1*S*,2*S*-*trans*-2-methylstyrene oxide in murine epoxide hydrolase was performed by using the following procedure. The molecular mechanics program CHARMM (version 25b2)[30] was used for these calculations utilizing MSI parameters, included in the program QUANTA,[31] for the amino acids and substrate. ChelpG charges from a HF/6-31+G(d,p) calculation were used for tMSO.[32] The crystal structure of murine epoxide hydrolase containing the inhibitor *N*-cyclohexyl-*N*′-(4-iodophenyl)urea (CIU) (PDB entry 1EK1) was used as the basis for the conformation of tMSO in the active site.[33] The phenyl ring of tMSO was overlayed onto the aromatic or aliphatic ring of the inhibitor CIU in the enzyme. The inhibitor was removed from the coordinate sets and the potential energy of the system was minimized by using a combination of steepest descents (SD, 500 steps) and adopted-basis Newton−Rapheson (ABNR, 1000 steps) methods with all the non-hydrogen atoms of the enzyme fixed.[30] The minimized coordinates were subjected to a second energy minimization in which all non-hydrogen atoms of the enzyme were constrained with a harmonic potential using a force constant of 1 kcal/(mol·Å^2) (500 steps of SD and 10000 steps of ABNR).

Results and Discussion

Noncatalyzed Reaction. The numbering system shown in Figure 1 for the reactants will be used in the discussion. The reaction involves formation of an ester intermediate via backside S_N2 attack by the carboxylate of Asp333 at either carbon center of the oxirane. The O1 of acetate is defined as that carboxylate oxygen which is closest to the tMSO carbon undergoing S_N2 attack. To avoid confusion, the transition state and product

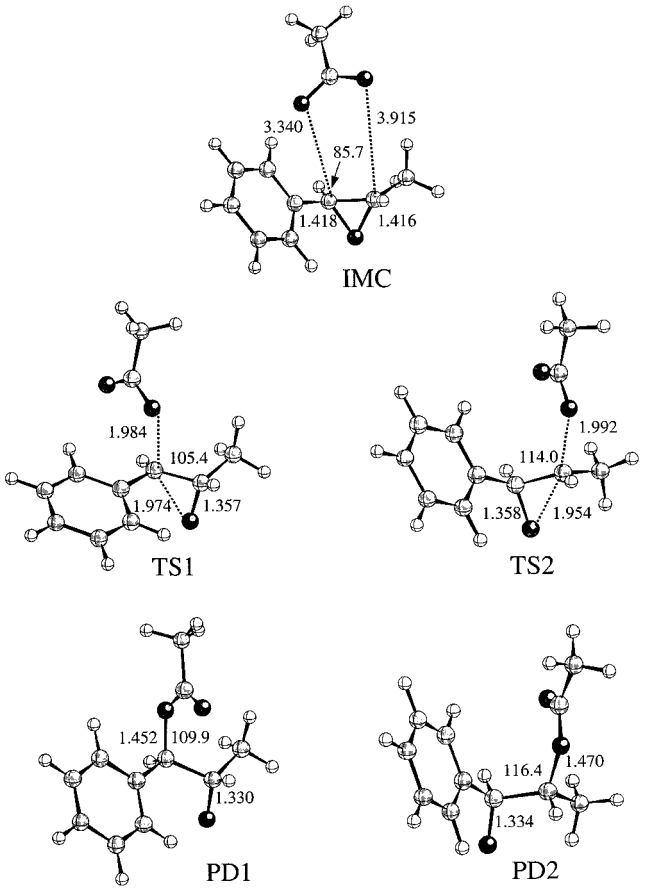

Figure 2. Stationary points obtained between acetate and tMSO at the HF/6-31+G(d,p) level of theory. The distances between atoms are in angstroms and the angles are in degrees. The angle reported in the IMC, TS1, and PD1 is formed by O1−C1−C2. The angle reported in TS2 and PD2 is formed by O1−C2−C1.

obtained from nucleophilic attack by acetate at C1 of tMSO will be referred to as TS1 and PD1, respectively. The transition state and product from C2 attack by acetate are denoted TS2 and PD2, respectively (Figure 2). In the calculations of noncatalyzed reactions, the lowest energy structure was the ion−molecule complex (IMC, see Table 1). In both the HF/6-31+G(d,p) and DFT (B3LYP/6-31+G(d,p)) optimized geometries for the IMC, the closest contact between the acetate and tMSO is between O1 and C1. The separations between these two atoms are 3.340 and 3.299 Å from HF and DFT calculations, respectively (Figure 2). Only the HF structures are shown in Figure 2, the calculated DFT structures are very similar (Supporting Information). The other oxygen of acetate forms a weaker interaction with the C2 atom of the epoxide. The distance between the atoms (O2−C2) is almost identical, 3.915 and 3.902 Å, from the HF and DFT calculations, respectively. A central barrier separates the reactants from the product (Figure 3). At the HF level of theory, the activation barrier from the IMC to the transition state is 32.6 kcal/mol when the acetate O1 attacks C1 of tMSO (Figure 3A). The barrier is 28.8 kcal/mol when the ring opening occurs at the C2 of tMSO (Figure 3B).

It is likely that electron correlation makes a contribution to the energetics of these structures due to the phenyl substituent on C1 of the epoxide. Two different calculations were performed to assess electron correlation effects. The optimized DFT stationary points include correlation effects, and single-point MP2/6-31+G(d,p) calculations were performed on the HF stationary points. The activation barriers for acetate attack at either C1 or C2 are in good agreement using these two different

(27) Mineva, T.; Russo, N.; Sicilia, E. *J. Comput. Chem.* **1998**, *19*, 290−299.
(28) Barone, V.; Cossi, M.; Tomasi, J. *J. Chem. Phys.* **1997**, *107*, 3210−3221.
(29) Stewart, J. J. P. *J. Comput. Chem.* **1989**, *10*, 209−220.
(30) Brooks, B. R.; Bruccoleri, R. E.; Olafson, B. D.; States, D. J.; Swaminathan, S.; Karplus, M. *J. Comput. Chem.* **1983**, *4*, 187−217.
(31) *QUANTA*: Molecular Simulations Inc.: San Diego, CA. 1998
(32) Breneman, C. M.; Wiberg, K. B. *J. Comput. Chem.* **1990**, *11*, 361−373.
(33) Argiriadi, M. A.; Morisseau, C.; Goodrow, M. H.; Dowdy, D. L.; Hammock, B. D.; Christianson, D. W. *J. Biol. Chem.* **2000**, *275*, 15265−15270.

Table 1. Energies for the Noncatalyzed Nucleophilic Addition of Acetate to tMSO

	electronic energy[a]	ZPE[b]
HF/6-31+G(d,p)		
acetate	−227.2542076	28.92
tMSO	−421.4920331	99.89
IMC	−648.7670543	129.33
TS1	−648.7146062	128.98
TS2	−648.7203415	128.81
PD1	−648.7442881	130.47
PD2	−648.7456787	130.34
MP2/6-31+G(d,p)//HP/6-31+G(d,p)		
acetate	−227.9202752	
tMSO	−422.9406215	
IMC	−650.8883557	
TS1	−650.8548165	
TS2	−650.8537173	
PD1	−650.8686703	
PD2	−650.8760473	
B3LYP/6-31+G(d,p)		
acetate	−228.5434743	29.51
tMSO	−424.1996662	102.32
IMC	−652.7645312	132.29
TS1	−652.7320581	131.88
TS2	−652.7303406	131.84
PD1	−652.7381398	133.07
PD2	−652.7449203	133.94
B3LYP/6-31+G(d,p) + COSMO		
acetate	−228.659539	
tMSO	−424.213247	
IMC	−652.857031	
TS1	−652.825185	
TS2	−652.820914	
PD1	−652.851271	
PD2	−652.854681	

[a] Values are in hartrees. [b] Values are in kcal/mol.

methods (Figure 3). Nucleophilic attack at C1 by acetate has an activation barrier of 20.7 and 20.0 kcal/mol from MP2 and DFT calculations, respectively. Attack at the C2 of the oxirane has a similar barrier height as C1 attack. The activation barrier for C2 attack was 21.2 and 21.0 kcal/mol from the MP2 and DFT calculations, respectively. Electron correlation lowers both activation barriers for formation of the ester. The activation barrier for C1 and C2 attack by acetate is reduced by almost 13 and 8 kcal/mol relative to the HF values, respectively. The separation between O1 and C1 in TS1 is 1.984 Å from the HF calculation; the separation is slightly shorter in the DFT calculation (1.970 Å). In TS2, the O1 to C2 distance is 1.992 and 1.997 Å for the HF and DFT structures, respectively. The C−O epoxide bond associated with the carbon under nucleophilic attack is elongated in both HF transition states (Figure 2). The DFT calculations predict even greater C−O epoxide bond breaking for TS1 and TS2 than in the HF structures, 2.019 and 1.976 Å, respectively. From the exothermicity of the reverse reaction a late TS in the forward reaction is expected. The calculated MP2 and DFT ester products are energetically not far below their associated transition state. PD2 is predicted to be more stable than PD1 at both levels of theory because the phenyl group next to the anionic oxygen is able to delocalize the net charge.

Noncatalyzed Reaction in Solution. An estimate of aqueous solvation effects on a reaction can be obtained by using a polarizable continuum model (PCM). The COSMO (CPCM) solvation model was used to estimate the effect of aqueous solvation on the S_N2 ester formation reaction. Single-point COSMO calculations utilizing the optimized gas-phase DFT geometries were used to obtain the energetics of these molecules in aqueous solution. The effect of solvation on this reaction

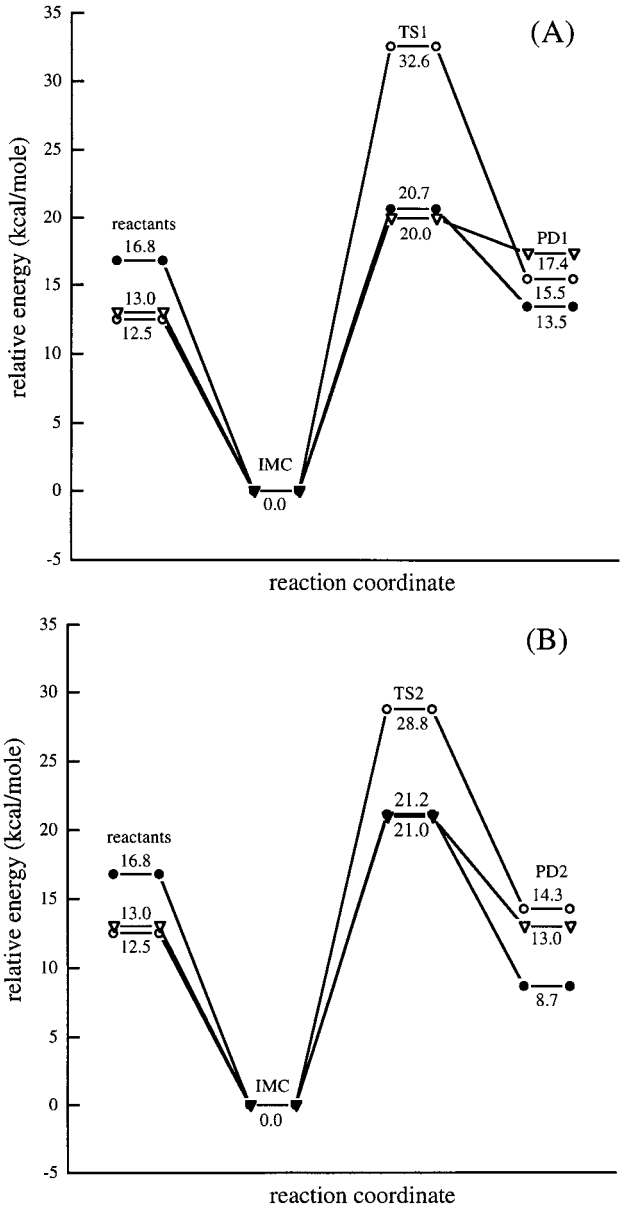

Figure 3. Relative energies for the noncatalyzed ring-opening reaction between acetate and tMSO at the HF/6-31+G(d,p) [○], MP2/6-31+G(d,p)//HF/6-31+G(d,p) [●], and B3LYP/6-31+G(d,p) [▽] levels of theory. Panel A shows the relative energies for acetate attack at the C1 of tMSO and Panel B shows the relative energies for C2 attack.

changes the relative energetics of the reactants and products. Inclusion of solvation effects causes the separated reactants to be lowest in energy (Table 1). The activation barrier in the gas phase for this ester reaction increases from 20.0 and 21.0 kcal/mol for C1 and C2 attack, respectively, to 29.9 and 32.5 kcal/mol in solution (Figure 4). Much of the increase in the activation barrier comes from the requirement to desolvate the acetate prior to its reaction. The IMC and transition states are not as well solvated even though they are anionic because the net charge is more distributed in the molecule (complex). Both products are more stable in solution than in the gas phase, although the reaction is still predicted to be endothermic. The experimental activation barrier for noncatalyzed ester formation between acetate and propene oxide in aqueous solution is 18.5−19.0 kcal/mol.[34,35] The experimental activation barrier is an average value

(34) Isaacs, N. S.; Neelakantan, K. *Can. J. Chem.* **1968**, *46*, 1043−1046.
(35) Biggs, J.; Chapman, N. B.; Wray, V. *J. Chem. Soc. B* **1971**, *55*, 66−71.

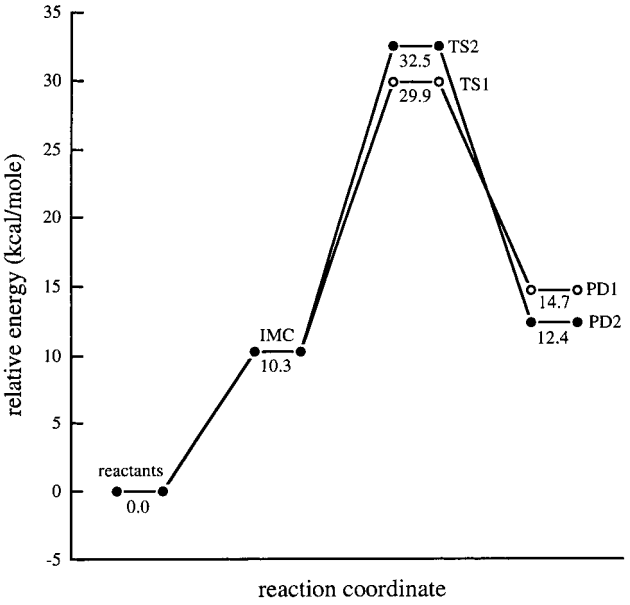

Figure 4. Relative energies for the noncatalyzed ring-opening reaction between acetate and tMSO in solution. The relative energies were obtained at the COSMO+B3LYP/6-31+G(d,p)//B3LYP/6-31+G(d,p) level of theory.

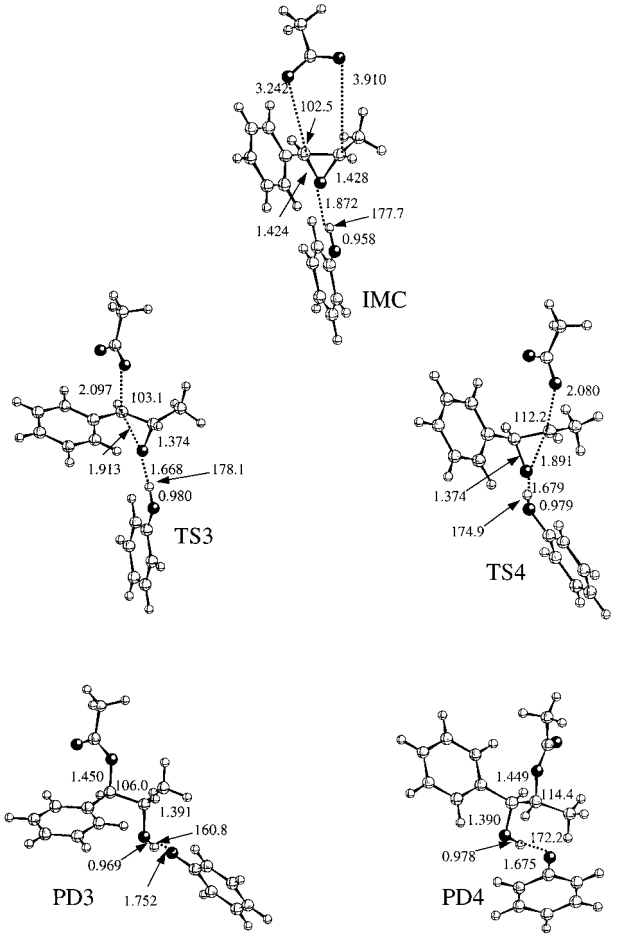

Figure 5. Stationary points obtained for the acid-catalyzed ring-opening reaction of tMSO from nucleophilic addition of acetate at the HF/6-31+G(d) level of theory. All distances are in angstroms and angles are in degrees. The angle reported between phenol and tMSO in all the structures is formed by the epoxide oxygen−hydroxyl hydrogen−hydroxyl oxygen (O−H−O). The angle reported between acetate and tMSO for the IMC, TS3, and PD3 is formed by O1−C1−C2. The angle reported between acetate and tMSO for TS4 and PD4 is formed by O1−C2−C1.

from data for attack at both carbons. The activation barrier for tMSO ring opening by acetate attack will be even higher since the additional phenyl group attached to the epoxide will increase the stability of the molecule and both reactive carbon centers are now secondary carbons. The calculated activation barrier for this reaction is reasonable, although it should be regarded as an upper limit. Specific interactions between water molecules and the complexes likely lowers the calculated activation barriers by stabilizing the negative charge developing on the epoxide oxygen during the reaction.

General-Acid-Catalyzed Reaction. The transition state and product formed from general-acid-catalyzed acetate attack at C1 of tMSO will be denoted TS3 and PD3, respectively. TS4 and PD4 will be used to denote the transition state and product from attack at C2 (Figure 5). A reaction barrier of ∼21 kcal/mol, as found in the noncatalyzed reaction, would be relatively high for an enzymatic reaction. In soluble epoxide hydrolases, there are two active site tyrosines which catalyze the hydrolysis reaction. Studies of mutants of murine and *Agrobacterium radiobactor* epoxide hydrolases have shown that one of the tyrosines can be replaced with a phenylalanine without loss of catalytic activity.[8,9] The kinetic effect of changing one tyrosine to a phenylalanine amounts to only a 1 to 2 kcal increase in $\Delta G^{\ddagger}$ for epoxide ring opening.

For computational simplicity and since the enzyme is catalytically competent with one tyrosine, a single phenol was used as the general-acid catalyst in these ab initio calculations (Figure 5). With phenol as the general-acid catalyst the activation barrier for this epoxide ring opening is significantly reduced (Figure 6) and formation of product becomes exothermic (Table 2). At the HF level, there is a 21.5 and 20.5 kcal/mol barrier separating the reactants from the products for C1 and C2 attack, respectively. This is approximately 10 kcal/mol lower than the HF activation barrier without the phenol general-acid catalyst. Inclusion of the acid catalyst in the calculation only slightly affects the geometry of the IMC. The distance between O1 and C1 is reduced from 3.340 to 3.242 Å for the noncatalyzed (HF structure) relative to the catalyzed reactions, respectively, and the C2 to O2 distance for this geometry is almost unaffected (3.910 and 3.915 Å for the catalyzed and noncatalyzed structures, respectively).

Electron correlation effects were assessed by single-point calculations at the MP2/6-31+G(d,p) and B3LYP/6-31+G(d,p) levels of theory on the HF geometries. Interestingly, the MP2 and DFT calculations predict almost identical activation barriers for oxirane ring opening. The MP2 and DFT activation barrier for nucleophilic attack at C1 by acetate is 10.4 and 9.2 kcal/mol, respectively (Figure 6A). The activation barrier for C2 attack is of similar height to C1 attack, 11.3 and 10.8 kcal/mol from MP2 and DFT calculations, respectively (Figure 6B). The central barrier for the general-acid-catalyzed reaction is in the same range of values obtained for the experimental activation energy for the acid-catalyzed methanolysis of propene oxide (13.4 kcal/mol).[35] This calculated activation barrier for tMSO ring opening is also similar to the barrier calculated by Laitnan, Rouvinen, and Peräkylä for the formic acid-catalyzed ring opening of propene oxide undergoing nucleophilic attack by formate at the primary carbon.[24] Their MP2/6-31+G(d,p) calculated activation barrier is 10.0 kcal/mol and their DFT (B3LYP/6-31+G(d,p)) calculations predicted an even lower barrier (6.7 kcal/mol). By utilizing the acidic hydrogen of tyrosine, the epoxide hydrolase is able to greatly reduce the activation barrier for forming the ester intermediate. Not

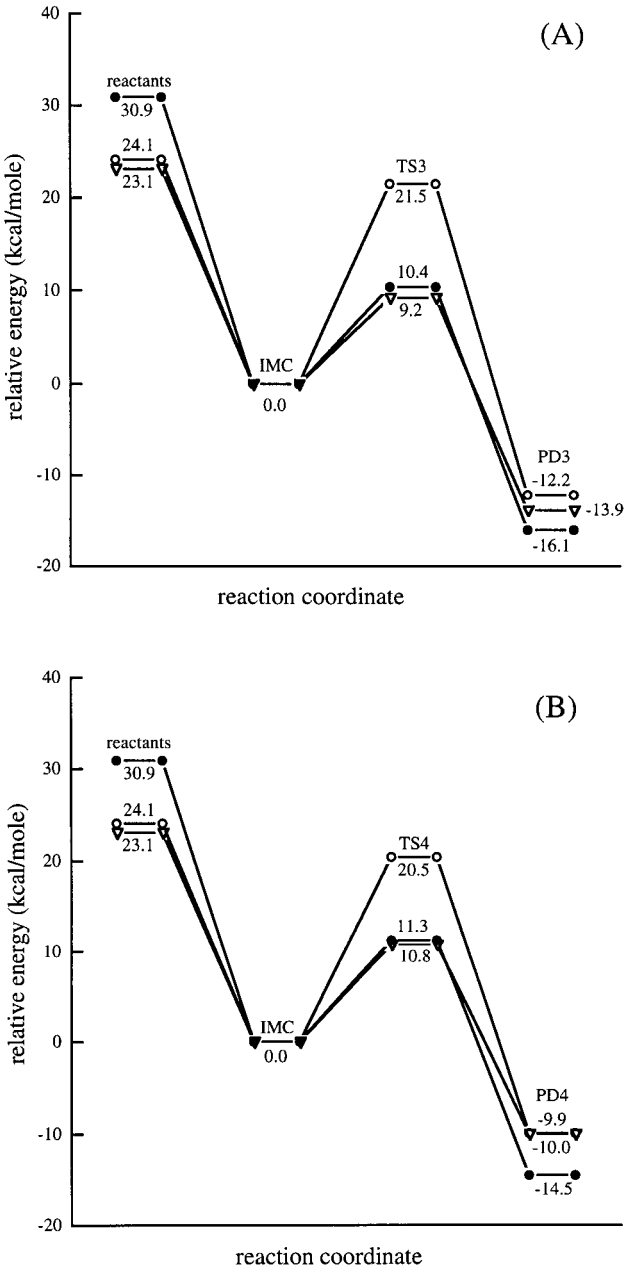

Figure 6. Relative energies for the acid-catalyzed ring-opening reaction of tMSO at the HF/6-31+G(d) [○], MP2/6-31+G(d,p)//HF/6-31+G(d) [●], and B3LYP/6-31+G(d,p)//HF/6-31+G(d) [▽] levels of theory. Panel A shows the relative energies for attack at C1 of tMSO by acetate. The relative energies for attack at C2 of tMSO by acetate are shown in Panel B.

surprisingly it has been shown that the rates of nucleophilic water attack with oxirane ring opening for styrene oxide and *trans*-methylstyrene oxide are subject to H_3O^+ catalysis.[36−38]

General-acid catalysis significantly affects the geometry of the transition states. With phenol as the general-acid catalyst, the calculated transition states for nucleophilic attack at both carbon centers of tMSO are earlier. The C1−O1 bond length in the transition state increases from 1.984 Å (TS1, HF) to 2.097 Å (TS3) with catalyst, and the C2−O1 bond length increases from 1.992 Å (TS2, HF) to 2.080 Å (TS4) with catalyst (Figures 2 and 5). The earlier transition state is expected on the basis of the greater stability of the product. The hydrogen bond between the phenol and epoxide oxygen contracts going from the IMC to either transition state (Figure 5). In the IMC, the H−O bond of the phenol is 0.958 Å and the distance from the epoxide oxygen to the acidic hydrogen is 1.872 Å. Both transition states have a slightly longer H−O bond relative to the IMC, 0.980 and 0.979 Å for C1 and C2 attack, respectively. There is a significant reduction in the distance between the epoxide oxygen and the phenolic hydrogen in the transition state. The separation goes from 1.872 Å in the IMC to 1.668 and 1.679 Å for C1 and C2 attack, respectively. The products consist of phenolate and neutral ester.

Experimental studies by Hine and co-workers with 1,8-biphenylenediol as a catalyst for epoxide hydrolysis may be considered (Scheme 2).[39,40] The rate of reaction is much greater than would be expected from the pK_a of this diphenol as predicted from the Brønsted plot for phenol catalysts. Ab initio calculations by Omoto and Fujimoto have shown that the activation barrier for the acid-catalyzed ring opening of oxirane reacting with ammonia (nucleophile) differs significantly de-

Table 2. Energies for the Acid Catalyzed Nucleophilic Attack of tMSO by Acetate

	electronic energy[a]	ZPE[b]
HF/6-31+G(d)		
acetate	−227.2495074	29.09
tMSO	−421.4717649	100.30
phenol	−305.5683552	62.79
IMC	−954.3305189	193.72
TS3	−954.2953456	193.17
TS4	−954.2973325	193.41
PD3	−954.3525597	195.40
PD4	−954.3489101	195.33
MP2/6-31+G(d,p)//HF/6-31+G(d)		
acetate	−227.9202752	
tMSO	−422.9405925	
phenol	−306.5955261	
IMC	−957.5081423	
TS3	−957.4906767	
TS4	−957.4895661	
PD3	−957.5364184	
PD4	−957.5338020	
B3LYP/6-31+G(d,p)//HF/6-31+G(d)		
acetate	−228.5414556	
tMSO	−424.1967154	
phenol	−307.4923457	
IMC	−960.2697726	
TS3	−960.2542721	
TS4	−960.2520280	
PD3	−960.2918361	
PD4	−960.2882994	

[a] Values are in hartrees. [b] Values are in kcal/mole.

Scheme 2

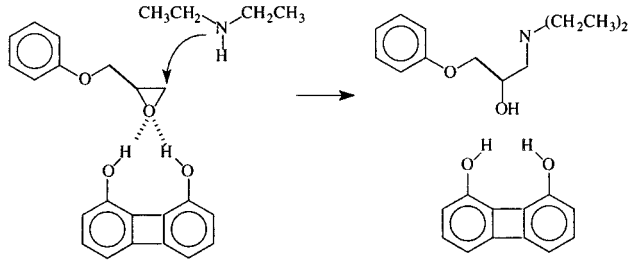

(36) Blumenstein, J. J.; Ukachukwu, V. C.; Mohan, R. S.; Whalen, D. L. *J. Org. Chem.* **1993**, *58*, 924−932.
(37) Lin, B.; Whalen, D. L. *J. Org. Chem.* **1994**, *59*, 1638−1641.
(38) Mohan, R. S.; Gavardinas K.; Kyere, S.; Whalen, D. L. *J. Org. Chem.* **2000**, *65*, 1407−1413.
(39) Hine, J.; Linden, S.-M.; Kanagasabapathy, V. M. *J. Am. Chem. Soc.* **1985**, *107*, 1082−1083.
(40) Hine, J.; Linden, S.-M.; Kanagasabapathy, V. M. *J. Org. Chem.* **1985**, *50*, 5096−5099.

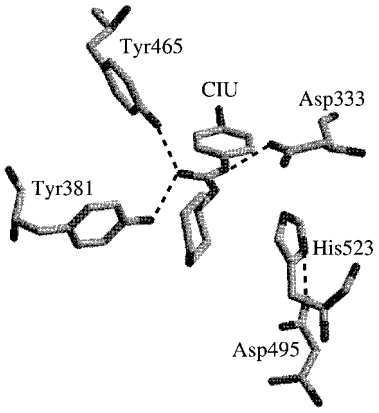

Figure 7. Binding geometry of *N*-cyclohyexyl-*N*′-(4-iodophenyl)urea (CIU) in the active site of murine epoxide hydrolase (PDB entry 1EK1). This figure was made with the program Raster3D.[49]

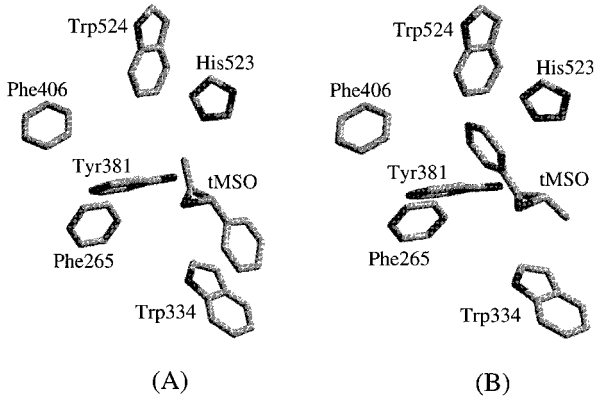

Figure 9. Interactions between the phenyl group of tMSO and aromatic residues in the active site. Only the side chains of the residues are shown in panels A and B.

pending on whether the reaction is catalyzed by a phenol or by 1,8-biphenylenediol.[41] The reaction when catalyzed by phenol has an activation barrier of 27.5 kcal/mol from MP2/6-311++G(d,p)//B3LYP/6-31G(d) calculations. The barrier is reduced by almost 7.5 kcal/mol when the same reaction is catalyzed by 1,8-biphenylenediol. The kinetics data for wild-type and mutant epoxide hydrolases indicate the amount of energy stabilization provided by the two tyrosines is not as great as is exhibited by 1,8-biphenylenediol in epoxide ring opening in the solvent butanone.

Binding Geometry of tMSO in Murine Epoxide Hydrolase. The crystal structure of murine epoxide hydrolase containing the inhibitor *N*-cyclohexyl-*N*′-(4-iodophenyl)urea (CIU)[33] suggests that 1*S*,2*S*-*trans*-2-methylstyrene oxide can be bound in the active site in two different conformations (Figure 7). The active site for this enzyme is very large, allowing it to bind structurally diverse substrates. Figure 8 shows two possible binding conformations for tMSO based on the epoxide hydrolase crystal structure 1EK1 and molecular mechanics energy minimization. Both conformations for tMSO in the active site of murine epoxide hydrolase are able to form hydrogen bonds between the oxygen of the epoxide and the catalytic tyrosines (Tyr381 and Tyr465).

When tMSO is in conformer A, the phenyl group of the epoxide is able to stack with the indole of Trp334 (Figure 9A). This interaction would enhance the ability of the benzyl carbon of the epoxide to stabilize an increase in positive charge at this position. When tMSO is in conformer B, the phenyl group is directed into an area surrounded by aromatic residues (Figure 9B). The side chains of Phe265, Tyr381, Phe406, His523, and Trp524 form a hydrophobic pocket in the active site large enough to bind a phenyl or cyclohexane group. The phenyl ring of tMSO is rotated approximately 90° in conformer A relative to conformer B. Asp333, Tyr381, and Tyr465 are well positioned to react with the oxirane in either tMSO conformation. Little perturbation in the active site of the enzyme is necessary to accommodate tMSO in either conformation. These two static geometries appear to favor formation of different products by the positioning of the Asp333 relative to tMSO. The near attack conformer (NAC)[42,43] formed in Figure 8B would lead to an ester on the phenyl side of the oxirane since OD1 of Asp333 is only 2.89 Å from C1 of tMSO. It should be kept in mind that proteins possess a high degree of structural plasticity and the active site is not a rigid entity, protein motions can be observed in molecular dynamics simulations and NMR experiments.[44,45] Therefore methyl side attack in this conformation is not precluded, but it is not as likely unless a significant change in conformation occurs between the oxirane and Asp333. Methyl side attack on tMSO can easily occur in conformer A; OD1 of Asp333 is positioned 2.96 Å from C2 of tMSO. Unlike the IMC in the gas-phase calculations, the other carboxylic oxygen (OD2) does not interact with the nonreacting carbon center of tMSO (see Scheme 3). The carboxylate of Asp333 is rotated approximately 180° (dihedral formed by O2−O1−C1−C2 in the IMC) relative to acetate in the gas-phase calculations placing the OD2 of Asp333 5.15 Å from C2 of tMSO in conformer A. In conformer B, the OD2 to C1 distance is 4.75 Å. OD2 of Asp333 for both conformers is hydrogen bonded to the backbone amide of Phe265. This is intriguing since the lack of interaction

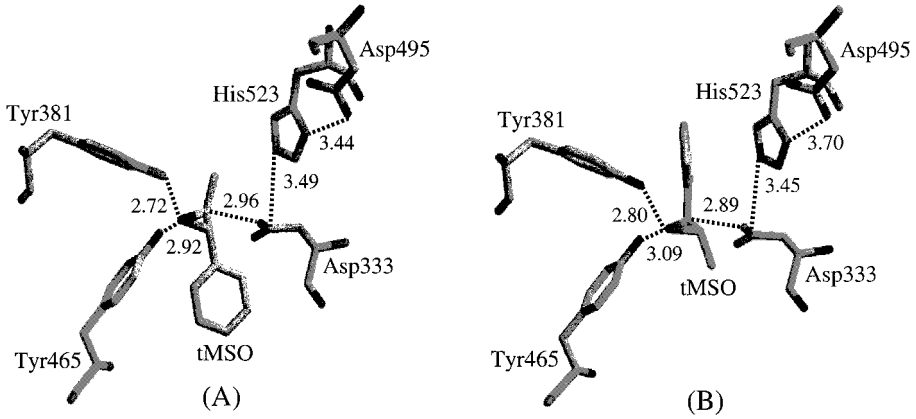

Figure 8. Possible binding geometries for tMSO in the active site of murine epoxide hydrolase based on the crystal structure 1EK1 and molecular mechanics calculations. The structures are denoted as conformers A and B in the text.

Scheme 3

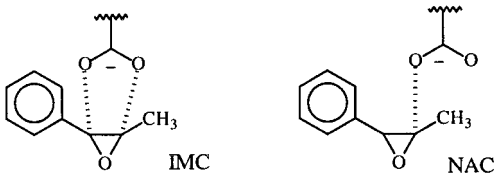

between OD2 of Asp333 and C2 of tMSO would lower the interaction energy between the reactants, thus destabilizing the ground-state NAC structure. It has been shown for catechol *O*-methyltransferase and haloalkane dehalogenase that the protein matrix prevents the reactants from forming the most stable structure possible in favor of the reactive NAC,[46,47] thereby destabilizing the ground state and reducing the activation barrier of the reaction. A better understanding of the conformation of the substrate in the active site of this epoxide hydrolase would come from performing a molecular dynamics study with tMSO in the two different conformations put forth and observing the resulting geometries.

Conclusions

HF, MP2, and DFT calculations have shown the epoxide hydrolase is able to substantially lower the reaction barrier for oxirane ring opening by positioning a pair of tyrosines to hydrogen bond to the epoxide oxygen. The MP2 and DFT calculations of the noncatalyzed reaction predicted an activation barrier of approximately 20−21 kcal/mol for epoxide ring opening depending on the carbon center undergoing reaction. This reaction is not favorable and is endothermic. The aqueous continuum solvation calculations predict the S_N2 displacement on tMSO by acetate is a very slow reaction. General-acid catalysis by phenol lowers the activation barrier to ∼10 kcal/mol. The general-acid-catalyzed reaction is exothermic with an earlier transition state relative to the noncatalyzed reaction. These results are consonant with the results of Laitinen et al. for the simpler reaction of formic acid-catalyzed ring opening of propene oxide by formate.[24] Interestingly, formic acid induces an earlier transition state structure and the oxirane ring-opening reaction is more exothermic than observed in this study with use of the weaker acid phenol, but the calculated activation barriers from these two studies are comparable. The models utilized in this study are accurate for epoxide hydrolases. The calculated energy difference between the activation barriers for general-acid-catalyzed C1 and C2 attack of tMSO by acetate is in accord with experiment. MP2 and DFT predict the activation barrier for C1 attack to be 0.9 and 1.6 kcal/mol lower in energy than that for C2, respectively. Experimentally, soluble epoxide hydrolase hydrolyzes 97% of *trans*-1,3-diphenylpropene oxide at the C1 position.[48] From molecular mechanics calculations, it is speculated that 1*S*,2*S*-*trans*-2-methylstyrene oxide can bind in the active site of murine epoxide hydrolase in two different conformations. These two binding conformations likely lead to two different ester products because of the positioning of Asp333 relative to the oxirane. It cannot be determined from these calculations which conformation of tMSO is preferred in epoxide hydrolase.

Acknowledgment. This study is funded by the National Science Foundation (Grant MCB-9727937). The authors gratefully acknowledge computer time on UCSB's Origin2000 which is partially supported by grants from the National Science Foundation (Grant CDA96-01954) and Silicon Graphics Inc.

Supporting Information Available: The stationary points for the noncatalyzed reaction obtained from the B3LYP/6-31+G(d,p) calculations (PDF). This material is available free of charge via the Internet at http://pubs.acs.org.

JA0037724

(41) Omoto, K.; Fujimoto, H. *J. Org. Chem.* **2000**, *65*, 2464−2471.
(42) Bruice, T. C.; Lightstone, F. C. *Acc. Chem. Res.* **1999**, *32*, 127−136.
(43) Bruice, T. C.; Benkovic, S. J. *Biochemistry* **2000**, *39*, 6267−6274.
(44) McCammon, J. A.; Harvey, S. C. *Dynamics of Proteins and Nucleic Acids*; Cambridge University Press: Cambridge, 1987.
(45) Jardetzky, O.; Lefevre, J.-F. *FEBS Lett.* **1994**, *338*, 246−250.
(46) Kahn, K.; Bruice, T. C. *J. Am. Chem. Soc.* **2000**, *122*, 46−51.
(47) Lau, E. Y.; Kahn, K.; Bash, P. A.; Bruice, T. C. *Proc. Natl. Acad. Sci. U.S.A.* **2000**, *97*, 9937−9942.
(48) Borhan, B.; Jones, A. D.; Pinot, F.; Grant, D. F.; Kurth, M. J.; Hammock, B. D. *J. Biol. Chem.* **1995**, *270*, 26923−26930.
(49) Merritt, E. A.; Bacon, D. J. *Raster3D: Photorealistic Molecular Graphics*; Carter, C. W. J., Sweet, R. M., Eds.; Academic Press: New York, 1997; Vol. 277, pp 505−524.